# Plasma diagnostics applicable to CDS/SUMER observations from SOHO*

**B. N. Dwivedi and Anita Mohan**

Department of Applied Physics, Institute of Technology, Banaras Hindu University, Varanasi 221 005, India

*'Busy old fool, unruly Sun, Why dost thou thus?'*
from the Sun Rising
John Donne (1572–1631)

**A great deal of effort in recent years has gone into the development of spectroscopic techniques to probe the physical parameters of the solar atmosphere. In this review, we discuss the spectroscopic diagnostics in the UV and EUV wavelength regions to study solar plasma, the atomic processes involved, the recent observations made from space and a wealth of EUV observations with excellent spatial, spectral and temporal resolution obtainable from the Coronal Diagnostic Spectrometer (CDS) and the Solar Ultraviolet Measurements of Emitted Radiation (SUMER) instruments flown on board the Solar and Heliospheric Observatory (SOHO) satellite.**

ACCESS to images and spectra of the hotter plasma in the UV (ultraviolet), EUV (extreme-ultraviolet) and X-ray regions provided a major advance over the few coronal forbidden lines seen in the visible and enabled the cooler chromospheric and photospheric plasma to be seen in its proper perspective, as part of a total system. In this way space observations have stimulated new and important advances, not only in space but also in ground-based observations and theoretical modelling. In Figure 1 we present an X-ray image of the Sun obtained with the Soft X-ray Telescope (SXT) aboard the Yohkoh spacecraft on 15 September 1991 at 19:17UT. The UV and EUV spectra present a rich source of information on the nature of the solar corona and the principal means of understanding the underlying mechanisms. Line shifts and broadenings give information about the dynamic phenomena in the solar atmosphere and permit a measurement of heating processes (waves, turbulence, etc.). Well chosen line intensity ratios provide knowledge of plasma temperature, density and relative element abundances in the emitting source. Absolute intensities of lines corresponding to a large range of temperature give a differential emission measure for the region being viewed and, combined with other physical information, a solution of the density and temperature gradients in that region. The inference of plasma temperature $T_e$ and density $N_e$ structure from spectral line ratio diagnostics is a problem of universal importance for both laboratory

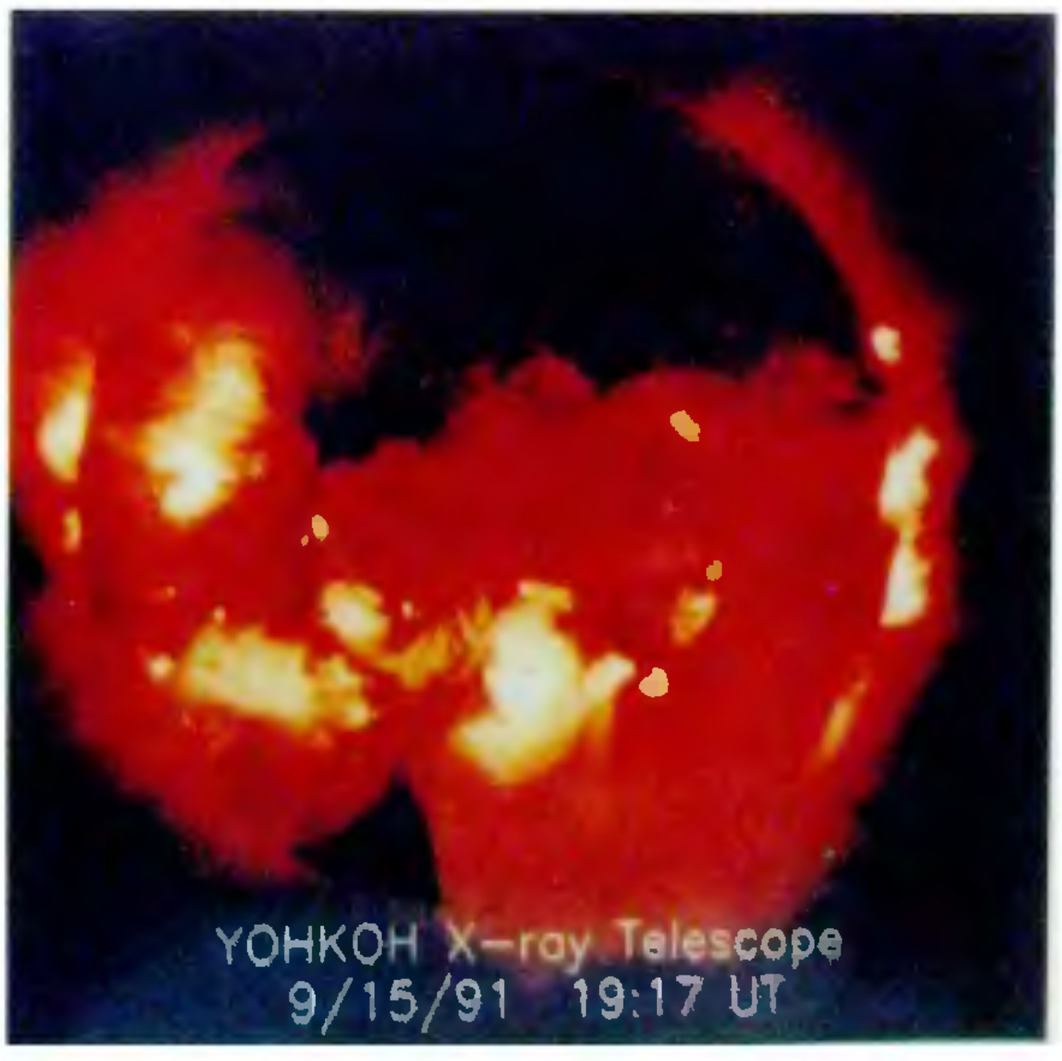


**Figure 1.** X-ray image of the Sun obtained with the soft X-ray telescope (SXT) aboard the Yohkoh spacecraft on 15 September 1991 at 19:17UT. In this soft X-ray image, the emissions are colour-coded, yellow for most intense to red for least intense. Active sunspot regions are marked by loops stretching high into the corona, while dark regions with sharp boundaries are coronal holes. (Courtesy: Yohkoh and the SXT team).

*In honour of Dr P. K. Raju, Indian Institute of Astrophysics, Bangalore on the completion of his 60 years.

and natural plasmas in both of which fields there exists a vast literature (see basic principles and reviews of the field in, for example, refs. 1–4). The physical importance of these diagnostics lies in the influence of the density and the temperature on the plasma process being considered, whether thermonuclear fusion, transport coefficients, energy transport, magnetic reconnection, particle acceleration, etc.

Because of its proximity, the high-temperature solar atmosphere is the only astrophysical plasma source that can be studied in great detail both because it can be to some extent spatially resolved, and because the high photon flux allows very high spectral resolution. The main source for our understanding of stellar atmospheres and even of low-density collisionally excited plasmas, such as supernovae, and their remnants is based on our knowledge concerning the plasma radiation processes in the solar atmosphere. Although some of these processes can be studied by high-resolution images of the atmosphere, much of our knowledge concerning temperature, density and dynamics of different regions of the solar atmosphere is obtainable through the technique of high resolution spectroscopy in the UV, EUV, and X-ray spectral regions. In addition, this part of the solar spectrum has shed light on certain problems of atomic physics and has been useful in understanding laboratory plasma spectra, such as those obtained from laser-produced and tokamak plasmas. In this review we mainly concentrate on the wavelength region 150–1610 Å (hereafter, we define it as the EUV region) which is excellently covered by the Coronal Diagnostic Spectrometer (CDS) and the Solar Ultraviolet Measurements of Emitted Radiation (SUMER) on Solar and Heliospheric Observatory (SOHO) satellite, successfully launched by an Atlas II-AS from Cape Canaveral Air Station on Saturday morning, December 2, 1995 at 08:08UT.

## Emission lines

The practical measurement of a spectral line intensity either in the laboratory or from a cosmic object requires the setting of a spectrometer with possibly a light collector (telescope) and detector. The signal measured by this system depends not only on the sensitivity of the system but also on properties of the source. It also depends on the extent to which the radiation is attenuated by the intervening space including re-absorption by the source itself (radiation trapping). Taking account of atomic excitation mechanisms, the line emissivity (per unit volume per unit time) for an optically thin spectral line is given by the expression:

$$\xi(\lambda_{ij}) = N_j A_{ji} \frac{hc}{\lambda_{ij}}, (j > i), (\text{erg cm}^{-3}\ \text{s}^{-1}), \quad (1)$$

where $A_{ji}$ is the spontaneous radiative transition probability, $h$ is Planck's constant, $c$ is the velocity of light, and $\lambda_{ij}$ is the wavelength for the transition $i$–$j$. $N_j$ is the number density of level $j$. Thus the atomic physics problem reduces to the calculation of the population density of the upper excited level $j$. For plasmas in LTE (local thermodynamic equilibrium), this is relatively simple and requires the application of the Saha–Boltzmann equation. Such plasmas are also liable to be optically thick and it is in taking account of this that the major problems of interpretation of spectral line intensities lie for LTE plasmas. The case of low density optically thin plasmas is treated here.

The number density $N_j$ can be further parameterized as

$$N_j(X^{+p}) = \frac{N_j(X^{+p})}{N(X^{+p})} \frac{N(X^{+p})}{N(X)} \frac{N(X)}{N(\text{H})} \frac{N(\text{H})}{N_e} N_e(\text{cm}^{-3}), \quad (2)$$

where $X^{+p}$ is the $p$th ionization stage of the element; $N_j(X^{+p})/N(X^{+p})$ is the population of level $j$ relative to the total $N(X^{+p})$ number density of ion $X^{+p}$ and is a function of the electron temperature and density; $N(X^{+p})/N(X)$ is the ionization ratio of ion $X^{+p}$ which is predominantly a function of temperature; $N(X)/N(\text{H})$ is the element abundance relative to hydrogen which varies in different astrophysical plasmas and also in different solar features; $N(\text{H})/N_e$ is the hydrogen abundance relative to electron density which is assumed to be ~0.8 for a fully ionized plasma. The flux at the Earth of a spectral line is given by:

$$I(\lambda_{ij}) = \frac{1}{4\pi R^2} \int_V \xi(\lambda_{ij}) dV \ \text{erg cm}^{-2}\ \text{s}^{-1}\ \text{sr}^{-1}, \quad (3)$$

where $V$ is the volume of emission and $R$ is Earth-to-object distance.

The collisional excitation processes are generally faster than ionization and recombination time scales in low density optically thin plasmas. Therefore, the collisional excitation is dominant over ionization and recombination in producing excited states. Thus the population density $N_j$ of the upper excited level $j$ must be calculated by solving the statistical equilibrium equations for a number of low-lying levels and taking account of all the important collisional and radiative excitation and de-excitation mechanisms:

$$N_j \left( N_e \sum_i C^e_{ji} + N_p \sum_i C^p_{ji} + \sum_{i>j} R_{ji} + \sum_{i<j} A_{ji} \right) = \sum_i N_i (N_e\ C^e_{ij} + N_p C^p_{ij}) + \sum_{i>j} N_i A_{ij} + \sum_{i<j} N_i R_{ij}, \quad (4)$$

where $C^e_{ij}$ and $C^p_{ij}$ are the electron and proton collisional excitation rate coefficients ($\text{cm}^3\ \text{s}^{-1}$), $R_{ji}$ the stimulated absorption rate coefficient ($\text{s}^{-1}$) and $A_{ji}$ the spontaneous radiation transition probability ($\text{s}^{-1}$).

There are some cases (e.g., optically allowed, electric dipole transitions) for which the assumption is made that

the population of the upper level of transition $j$ occurs mainly via collisional excitation from the ground level $i$ and that the radiative decay overwhelms any other depopulation process. This is called the coronal model approximation. The population of the upper level $j$ is negligible in comparison with the ground level $i$, which means $N_i(X^{+p})/N(X^{+p}) \simeq 1$. The statistical equilibrium equations can be solved as a two-level system for each transition:

$$N_i(X^{+p})N_e C_{ij}^e = N_j A_{ji}. \quad (5)$$

Substituting equations (2) and (5) into equation (1) and remembering that $N_i(X^{+p})/N(X^{+p}) = 1$, we get

$$\xi(\lambda_{ij}) = \frac{N(X^{+p})}{N(X)} \frac{N(X)}{N(\mathrm{H})} \frac{N(\mathrm{H})}{N_e} C_{ij}^e \frac{hc}{\lambda_{ij}} N_e^2. \quad (6)$$

Thus the line intensity, which is the integration of the line emissivity over the emitting volume, is given by

$$I(\lambda_{ij}) = \int_V G(T_e) N_e^2 \mathrm{d}V, \quad (7)$$

where $G(T_e)$ can be calculated from the ionization ratio, element abundance and atomic parameters. The electron density can be crudely deduced assuming that the spectral line is emitted over a homogeneous volume estimated from images in that line

## Plasma density and temperature diagnostics

The first question which one might justifiably ask is: why has so much effort been put into the development of electron density diagnostics? Obviously, the electron pressure ($N_e T_e$) is an important parameter in any theoretical model for the plasma, but why not simply deduce the electron density from the total line emission and an estimate of the emitting volume? This can and has been done in numerous analyses. However, this assumes a knowledge of the volume for the emission. If the spatial resolution for the observations were good enough and the emitting material was homogeneously distributed throughout the volume, then the electron density estimate (assuming a knowledge of element abundance and all the atomic parameters) would be reasonable. Solar plasma, however, is characterized by unresolved filamentary structures even with the best spatial resolution observations currently available. The determination of electron density from spectral line ratios from the same ion, makes no assumption about the size of the emitting volume, ionic fractions or the element abundance value, providing a powerful diagnostic for the plasma conditions.

Spectral lines may be grouped into different categories according to the behaviour of the upper level population: allowed lines collisionally excited from the ground level (e.g., coronal model approximation); forbidden or intersystem lines originating from a metastable level-$m$; and allowed lines excited from a metastable level. For the sake of simplicity, let us consider again a two-level model. The radiative decay rate is generally very small ($A_{mi} \simeq 1$–$100\ \mathrm{s}^{-1}$) for forbidden and intercombination transitions. In such cases the collisional de-excitation becomes an important depopulating mechanism ($A_{mi} \simeq N_e C_{mi}^e$) and may even be the dominant mechanism. Moreover, the population of the metastable level becomes comparable with the population of the ground level and we have

$$N_m = \frac{N_i N_e C_{im}^e}{N_e C_{mi}^e + A_{mi}}. \quad (8)$$

For small electron densities, $A_{mi} \gg N_e C_{mi}^e$, the line intensity has the same dependence on the density as an allowed line:

$$I(\lambda_{mi}) \simeq N_e^2.$$

For very large values of electron density, the collisional de-excitation dominates, that means $N_e C_{mi}^e \gg A_{mi}$, and the metastable level is in Boltzmann equilibrium with the ground level:

$$\frac{N_m}{N_i} = \frac{C_{im}^e}{C_{mi}^e} = \frac{\omega_m}{\omega_i} \exp\left(\frac{-\Delta E_{im}}{kT_e}\right). \quad (9)$$

In this case the line intensity has the form:

$$I(\lambda_{mi}) \simeq N_e.$$

For intermediate values of electron density, $A_{mi} \simeq N_e C_{mi}^e$; the population of the metastable level is significant and the line intensity varies as:

$$I(\lambda_{mi}) \simeq N_e^\beta,\ 1 < \beta < 2.$$

If the population of metastable level ($m$) is comparable with the ground level ($i$), then other excited levels ($j$) can be populated from this metastable level as well as from the ground level and the dependence of the intensity on electron density becomes:

$$I(\lambda_{jm}) \simeq N_e^\beta,\ 2 < \beta < 3.$$

Thus, if we compare ratios of spectral lines in different categories, we can determine the electron density of the emitting plasma. For most ions it is necessary to consider the atomic processes between several levels and solve the full statistical equilibrium equations.

The simplest but crudest method of deducing the plasma temperature is to assume ionization equilibrium[5,6]. Since many ions are formed over the same range of temperature, line ratios can be plotted as a function of temperature of the emitting isothermal plasma. A more accurate determination of electron temperature can be obtained from the intensity ratio of two allowed lines

excited from the ground level $i$ but with significantly different excitation energy. The ratio is given by:

$$\frac{I(\lambda_{ij})}{I(\lambda_{il})} = \frac{\Delta E_{ij}}{\Delta E_{il}} \frac{\gamma_{ij}}{\gamma_{il}} \exp\left(\frac{\Delta E_{il} - \Delta E_{ij}}{kT_e}\right). \quad (10)$$

Here $\gamma_{ij}$ is the thermally-averaged collision strength. The ratio is sensitive to the change in electron temperature if $(\Delta E_{il} - \Delta E_{ij})/kT_e \gg 1$, assuming that the lines are emitted by the same isothermal volume with the same electron density. Such spectral lines are far apart in wavelength and it may be necessary to use lines from different instruments. This gives rise to major uncertainties in the derived temperature due to the relative calibration of the intensities.

## Emission measure analysis

The emission measure is basically a measure of the amount of hot plasma as a function of temperature and it is the primary characteristic which any theoretical model should predict. The volume emission measure (EM) is defined as:

$$\mathrm{EM} = \int_V N_e^2 \, dV. \quad (11)$$

Following Pottasch[7], the contribution function over a temperature interval $\Delta T$, near the temperature $T_{max}$ of the peak of the contribution function $G(T_e, \lambda_{ij})$ for ion, gives the largest contribution of the emission. Assuming the emitting volume to be isothermal, and the elemental abundance known, one may determine a mean value of the emission measure from the observed line intensity:

$$I^{obs}(\lambda_{ij}) = \beta \frac{N(X)}{N(\mathrm{H})} \langle \mathrm{EM} \rangle \int_{\Delta T} G(T_e, \lambda_{ij}) \, dT, \quad (12)$$

where from equations (3) and (6), $\beta = (N(\mathrm{H})/N_e)(1/4\pi R^2)$.

This method is used to derive the isothermal $\langle \mathrm{EM} \rangle$ as a function of temperature using lines emitted at different values of $T_{max}$. This is illustrated in Figure 2 for the solar atmosphere.

In a more general formulation:

$$I^{obs}(\lambda_{ij}) = \beta \frac{N(X)}{N(\mathrm{H})} \int G(T_e, \lambda_{ij}) \, \phi(T) \, dT, \quad (13)$$

where $\phi(T) = N_e^2 dV/dT$ is called the differential emission measure (DEM) function and specifies the amount of material in the temperature interval $T$ and $T + \Delta T$. To derive the DEM from the observations, one must solve a set of integral equations[8]. A study of different integral inversion techniques to solve the DEM problem has recently been carried out by a SOHO : CDS and SUMER study group[9].

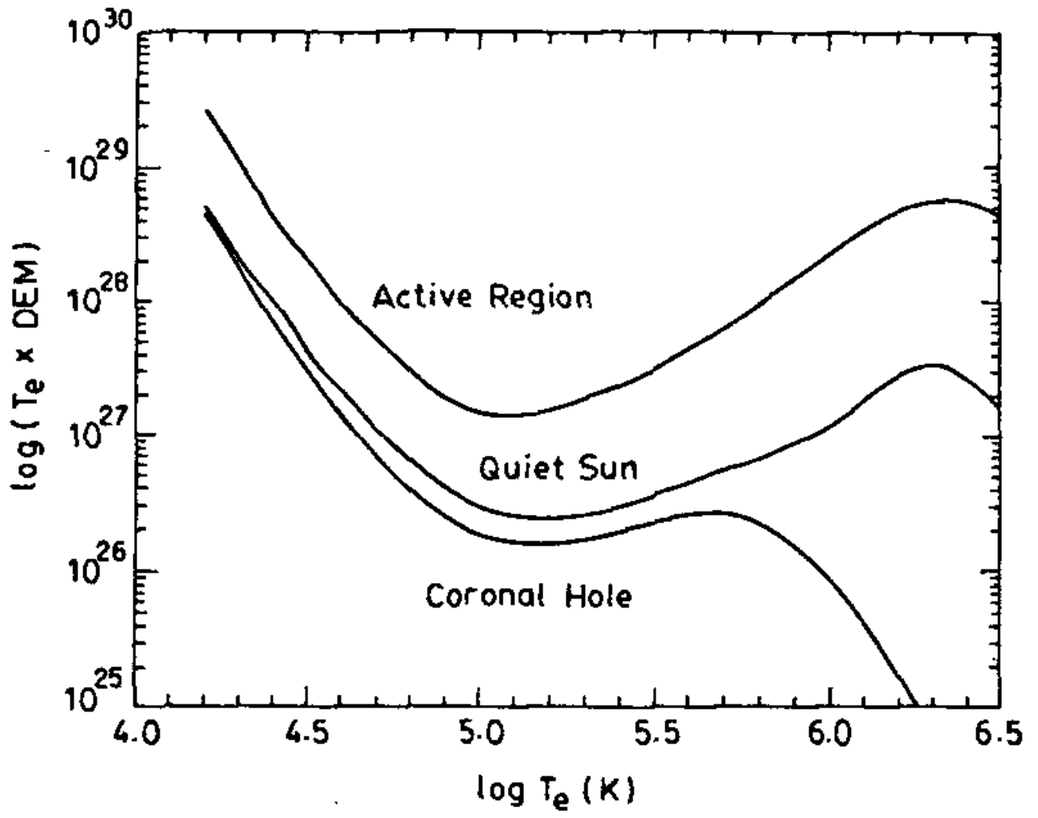


**Figure 2.** Emission measure for different solar regions[17].

## Abundance determination

One approach to determining element abundances is to use the detailed shape of DEM distribution for ions from the same element and apply an iterative procedure to normalizing the DEM curves for different elements. Pottasch[7] first used this technique in the UV to deduce abundances relative to silicon. The technique has recently been applied to solar spectra[10].

There is currently a great controversy raging over the element abundances in different regions of the solar atmosphere. Meyer[11–13] reviews the values for element abundances in both solar and cosmic plasmas. It appears that the element abundances in the solar wind differ from those in the photosphere. The variation depends on the value for the First Ionization Potential (FIP). In fact, it seems that the coronal abundances for certain types of regions (characterized by open field lines) differ from photospheric values. In the solar corona, the abundances of elements with low FIPs (< 10 eV) such as Fe, Si and Mg, are observed to be enhanced relative to elements with high FIPs (> 10 eV) such as O, Ne and Ar, by a mechanism which is currently not understood. This phenomenon is known as the 'FIP effect'. This is illustrated[14] in Figure 3. It should be noted that any element abundance variations can have important consequences for the radiative power loss functions[15,16].

## Spectral line profiles

Line shifts and broadenings give information about the dynamic nature of the solar and stellar atmospheres. The transition region spectra from the solar atmosphere are characterized by broadened line profiles. The nature of this excess broadening puts constraints on possible

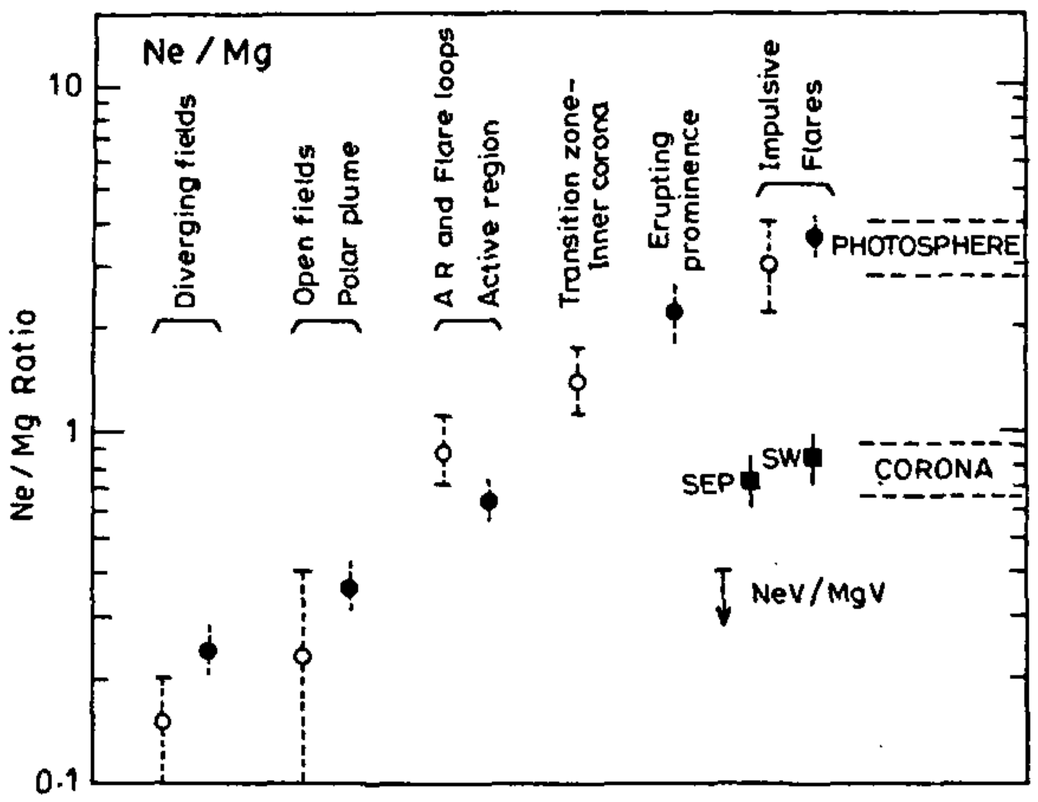


**Figure 3.** Relative element abundances of Ne/Mg for different types of solar regions[14]; the filled circles from a detailed EM analysis, open circles from estimates using the Ne VI/Mg VI line ratios. Solar energetic particle (SEP) and solar wind (SW) values are shown together with the abundance ratios in the photosphere and bulk corona.

heating mechanisms. Systematic red shifts in transition region lines have been observed in both solar spectra and stellar spectra of late type stars. On the Sun, outflows of coronal material have been correlated with coronal holes, a probable source of the solar wind. The excess broadening of coronal lines above the limb provides information on wave propagation in the solar wind.

If the optically thin spectral lines can be fitted with Gaussian profiles, the intensity per unit wavelength $I_\lambda$ is defined as:

$$I_\lambda = \frac{1}{\sqrt{2\pi\sigma}} \exp\left(-(\lambda-\lambda_0)^2 / 2\sigma^2\right), \tag{14}$$

where $I = \int I_\lambda \, d\lambda$ is the integrated intensity and $\sigma$ is the Gaussian width given by

$$\sigma^2 = \frac{\lambda^2}{2c^2}\left(\frac{2kT}{M} + \xi^2\right) + \sigma_I^2 \tag{15}$$

for a Maxwellian velocity distribution of temperature $T$, usually assumed to be the temperature corresponding to peak ionic concentration. Here $M$ is the mass, $\sigma_I$ is the Gaussian instrumental width and $\xi$ is the most probable non-thermal velocity[17].

## Solar observations from space

The EUV emission has been measured by a large number of space programs such as OSOs (Orbiting Solar Observatories), Skylab, SMM (Solar Maximum Mission) and Spacelab and by rocket-borne EUV spectrometers including SERTS (Solar EUV Rocket Telescope and Spectrograph: an EUV imaging spectrograph with high spectral and spatial resolution). We present a bird's eye view of major solar space programs in Table 1 and discuss very briefly about some of them mostly relevant to the CDS and the SUMER spectral range.

Very little observation is available in the wavelength region (100–170 Å) which is rich in spectral lines from the high temperature ($\geq 3 \times 10^6$ K) iron ions Fe XVIII–Fe XXIV. The only available flare spectra were obtained with the Goddard Space Flight Center (GSFC) grating spectrometer flown on OSO-5. Several density-sensitive line ratios fall in this wavelength region, particularly Fe XXI $\lambda$128.73/$\lambda$145.66 line ratio is useful for $N_e \geq 10^{11}$ cm$^{-3}$. The diagnostic potential of these spectra together with references to atomic calculations for the iron ions have been presented[18]. Theoretical diagnostic line ratios have recently been investigated[19] and a good agreement has been found with the UV spectra measured by the Princeton Large Toras tokamak. The Harvard College Observatory (HCO) instrument on OSO-4 and OSO-6 covered the wavelength range 300–1400 Å. Many spectral lines were observed and models of the chromosphere, transition region and corona were derived[20]. Observations in the 190–300 Å wavelength region were made with the GSFC spectroheliograph on the OSO-7 satellite. The emission lines from Fe IX–Fe XVI ($6 \times 10^5$–$2.5 \times 10^6$ K) were studied both on the disk and as a function of height above the limb. The emission from the Fe IX–Fe XIII lines fell sharply between the limb ($R/R_0 = \rho = 1$) and $\rho = 1.1$. In contrast, the Fe XIV and Fe XV lines were still strong out beyond $\rho = 1.3$ (ref. 21). The Fe XIII and Fe XIV line ratios were used to estimate electron densities in the range $10^8$–$10^{10}$ cm$^{-3}$. Density-sensitive line ratios from a range of other ions of iron, silicon and sulphur were studied[22]. The OSO-8 satellite carried instruments covering approximately the wavelength range 1000–2000 Å. With high spatial and spectral resolution, it was possible to study line broadenings and redshifts in the transition region and chromospheric lines. Results are published in the proceedings of the OSO-8 workshop[23]. The C IV 1548 Å emission was studied[24], considering both the line widths and profile symmetry properties in quiet regions (network and cell centre) and it was found that acoustic waves could not supply enough energy to balance radiative and conductive losses and that the data were consistent with heating by Alfven waves.

Many line diagnostics were developed using the UV and EUV spectra from Apollo Telescope Mount (ATM) instruments on board Skylab: the Naval Research Laboratory (NRL) slitless spectrograph SO82A (170–630 Å); the HCO UV spectrometer SO555 (280–1350 Å) and the

**Table 1.** EUV instruments covering the spectral range 150 to 1610 Å

| Satellite | Experiment | Spectral range (Å) | Spectral resolution (Å) (best) | Spatial resolutioon (arcsec)$^2$ |
|---|---|---|---|---|
| OSO-7 | GSFC Spectroheliograph | 190–300 | 0.42 | 20 × 60 |
| Skylab ATM | NRL SO82A UV slitless spectroheliograph | 170–630 | 0.1 | 2 × 2 |
| | NRL SO82B Slit spectrograph | 1170–3000 | 0.06 | 2 × 60 |
| | HCO SO555 | 280–1350 | 1.6 | 5 × 5 |
| SMM | UVSP (UV Spectrometer and Polarimeter) | 1150–3600 | 0.05 | 3 × 3 |
| Spacelab 2 rocket flights | HRTS (High Resolution Telescope and Spectrograph) | 1170–1700 | 0.05 | 1 × 1 |
| Rockets | LASP EUV Coronal Spectrometer | 605–635<br>1210–1270 | 0.003 | 20 × 60 |
| Spacelab 2 | CHASE (Coronal Helium Abundance Spacelab Experiment) | 150–1344 | 0.7 | 15 × 15 |
| SERTS | Solar EUV Rocket Telescope and Spectrograph | 170–450 | 0.005 | 7 × 7 |
| SOHO | CDS (Coronal Diagnostic Spectrometer) | 150–800 | ≤ 0.2 | 2 × 2 |
| SOHO | SUMER (Solar UV Measurements of Emitted Radiation) | 500–800<br>800–1610 | 0.04 first order<br>0.02 second order | 1.5 × 1 |

NRL slit spectrograph SO82B (970–3940 Å). Recent work of particular interest with SO82A spectra has focused on the determination of element abundances. This work has been reviewed[14,25,26]. These authors compare the intensities of the two lines Mg VI (400.67 Å) and Ne VI (401.14 Å) which have almost identical $G(T_e)$ functions ($T_{max} = 4 \times 10^5$ K), but very different FIP values. It was found that the Ne/Mg ratio is lower in open field regions than in closed field regions (see Figure 3). Such abundance variations are very important and have stimulated a great deal of discussion about the formation and acceleration of material at the base of the solar atmosphere. In view of its universal importance in understanding solar and stellar physics, a detailed theoretical study has been carried out for Ne VI/Mg VI line ratio diagnostics suitable for quiet Sun, active region, sunspot, and flare plasmas[27].

Spectroscopic diagnostics for boron-like ions have been extensively studied[28–34]. References to further diagnostic work on the boron, carbon, nitrogen and oxygen-like ions are given[3]. Beryllium-like ion C III is a useful diagnostic for the quiet Sun at lower densities. Recent theoretical emission line ratios for C III ion have been published[35]. The C III multiplet at ~1175 Å was studied[36] to indicate how opacity could affect the line intensity ratios within the multiplet and provide a method of determining the electron density. The range of electron density sensitivity for many transition region and coronal lines is given[1]. The forbidden coronal lines from Mg VI, Si VIII and S X ions were studied as electron density diagnostics in the inner corona[37–39]. Inhomogeneous structures in the emitting volume may affect the electron density diagnostic line ratio techniques. This problem was discussed for O IV and S X ions[40]. These ideas have been pursued in more detail for both isothermal[41] and non-isothermal plasmas[42,43]. The HCO UV spectrometer covered a very important wavelength range with strong spectral lines from the transition region and corona[44]. Unfortunately, although the spatial resolution was very good (5 arcsec), the spectral resolution was rather limited (1.6 Å). Nonetheless, several useful diagnostics were developed and studied[3].

## Solar EUV Rocket Telescope and Spectrograph

An EUV imaging spectrograph developed at the Goddard Space Flight Center has been used to obtain coronal observations with high spectral and spatial resolution[45]. The instrument SERTS (Solar EUV Rocket Telescope and Spectrograph) covers the wavelength region 235–450 Å (170–225 Å in second order) with a spectral resolution approaching 10,000. SERTS, which has been flown several times since 1989, produces both non-overlapping spectroheliograms and stigmatic spectra (slit 4.9' by 7") of the same solar region. A line identification list has been produced[46]. The temperature range covered is $4.7 \leq \log T_e \leq 6.8$ with lines from ions from He II (304 Å) to Ca XVIII. The SERTS spectra contain many useful diagnostic lines, in particular from the iron ions. The EUV spectral emission intensities for Fe IX–Fe XXIV have been recalculated, based on the most recent atomic data[47]. The predicted intensities with the SERTS values and also with the spectrum of Capella have been compared. The coronal temperature using SERTS intensities for different iron ion stages have

been studied[48]. The spectroscopic diagnostics for Ne VI, Mg VI, Si VIII and Mg VIII ions observed by SERTS have recently been investigated[49]. The spectra from the SERTS-3 rocket flight in 1989 have been used to study the He II line at 304 Å (ref. 50). In this study SERTS and X-ray data have been used to study the relative importance of the line formation processes for a weak flare and it was found that the photoionization–recombination mechanism certainly competes with and may even dominate electron excitation in the He II 304 Å line formation. Several ions from beryllium, boron, carbon, nitrogen and oxygen isoelectronic sequences in the temperature range $1.6 \times 10^5\ \mathrm{K} < T_e < 1.3 \times 10^6\ \mathrm{K}$ have been studied, making use of the SERTS observation to compute electron density, column emission measure, filling factor, relative element abundance variation, etc.[51].

## CDS and SUMER instruments on SOHO

The Coronal Diagnostic Spectrometer (CDS), spectral range 150–800 Å (ref. 52), and the Solar Ultraviolet Measurements of Emitted Radiation (SUMER), spectral range 500–1610 Å (ref. 53), have been flown on board the SOHO mission. These instruments will be able to address two fundamental goals of SOHO: why does the corona exist and how is it heated? and where and how are the solar wind streams accelerated? The CDS and SUMER instruments compliment each other very well, since CDS will rely heavily on diagnostics to determine physical parameters in the corona and SUMER will be able to study the dynamical aspects of the transition region and corona. Some of the prominent solar ions with their wavelengths and temperatures, covered by these instruments, are shown in Figure 4. We discuss here the diagnostic potentiality which the CDS and SUMER instruments are capable of making.

The CDS instrument consists of a Wolter II grazing incidence telescope feeding both a Normal Incidence Spectrometer (NIS) (stigmatic slit) (308–381 Å, 513–633 Å) and a Grazing Incidence Spectrometer (GIS) (151–221 Å, 256–338 Å, 393–493 Å, 656–785 Å). These bands have been carefully chosen to cover useful spectroscopic diagnostic lines. The NIS channels cover ions from a wide temperature range ($2 \times 10^4$ K–$6 \times 10^6$ K), including Mg IX 368 Å line which is very useful for studying coronal holes, the Fe XVI 335 Å and 361 Å lines which are very strong in active regions and the Fe XIX flare line at 592 Å. CDS should achieve a spatial resolution of 2 arcsec, a spectral resolution of $\Delta\lambda \leq 0.2$ Å, $\lambda/\Delta\lambda = 10^4$ and a temporal resolution of 1 second. Full details of the design, the scientific objectives, spectroscopic diagnostics and planned observing sequences are given, referred to as the CDS Blue Book[54].

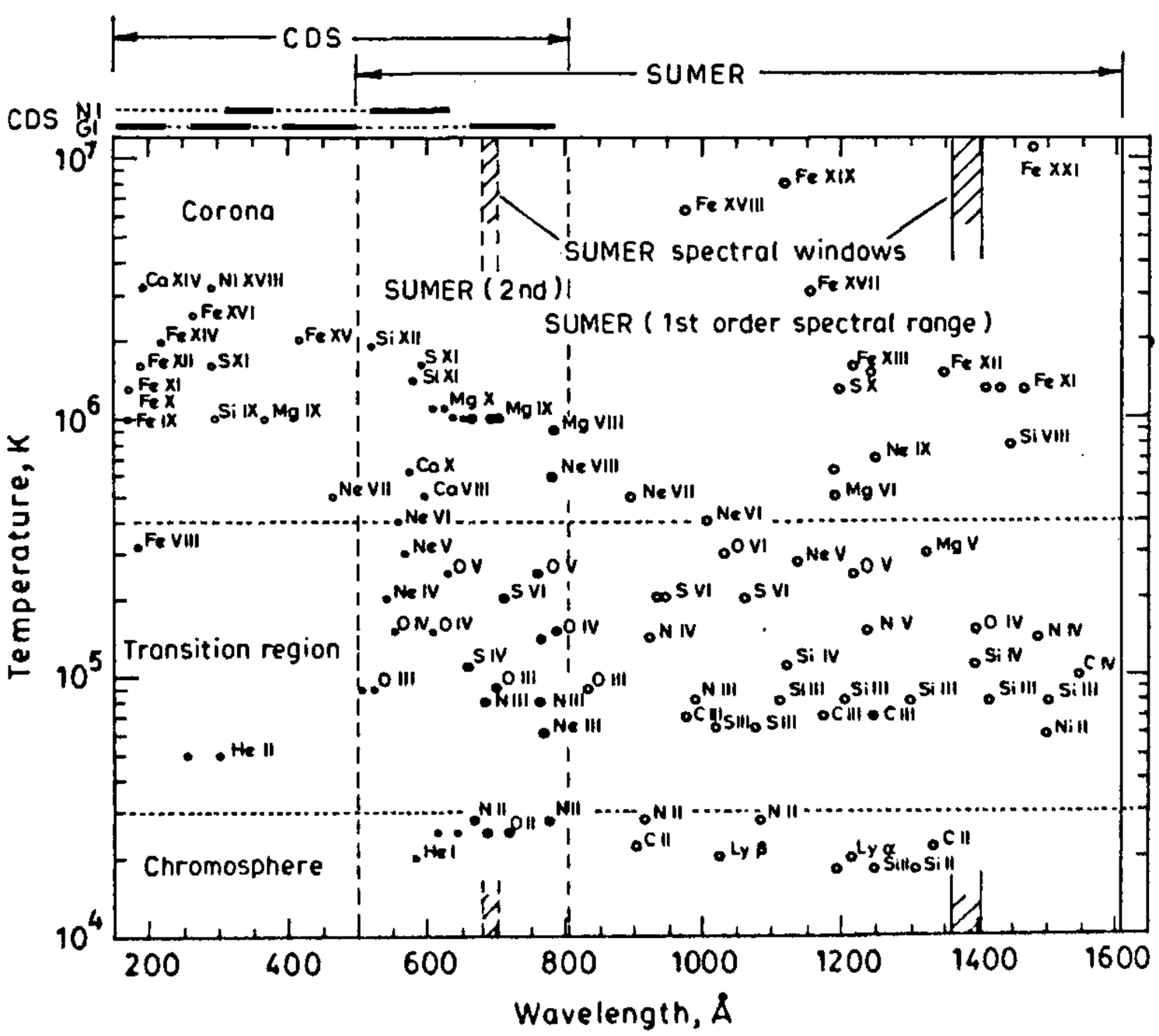


**Figure 4.** Prominent solar ions with their wavelengths and temperatures, covered by the CDS and SUMER instruments aboard the SOHO spacecraft, adapted from ref. 53.

The SUMER instrument is a normal incidence telescope stigmatic spectrometer. It covers the wavelength range 800–1610 Å in first order and 500–800 Å in second order in a 40 Å and 20 Å band respectively. SUMER will observe primarily transition region and chromospheric lines with a very high spectral resolution $\lambda/\Delta\lambda$ = 17700–38300 ($\Delta\lambda$ = pixel resolution element), a spatial resolution close to 1 arcsec and temporal resolution down to 1 second. SUMER will be able to detect velocities down to 1–3 km sec$^{-1}$ from line shifts. Details of the SUMER design, scientific objectives and planned observing sequences are given, referred to as the SUMER Red Book[55].

The CDS and SUMER instruments are designed to make extensive use of spectroscopic diagnostics for the determination of the physical parameters of the transition region and corona. A great deal of effort is going into the development of these techniques to ensure that they are accurate. This requires interfacing solar analysis programs with the best available atomic data calculations. This study covers electron density and temperature determination, differential emission measures, elemental abundance variations and basic atomic data, including both electron excitation, ionization and recombination. Many CDS spectral line pairs have been included for density and temperature diagnostics[54]. These have previously been studied from OSO, Skylab and more recently with SERTS observation. The boron-like ions provide very useful electron density diagnostics for a range of solar features; Mg VIII for coronal hole observations[32] and Si X for active regions[28,29]. The B-like, C-like, N-like and O-like ions have previously been studied. Other line ratios (e.g., from Ca XV, Ca XVI) could be very useful for flare or nano-flare electron density diagnostics[56].

Spectral lines in the SUMER spectral range have also been identified as useful electron density and temperature diagnostics[55]. If it is not possible to use spectral line ratios from the same ion, one can use the ratio of a forbidden line from one ion to an allowed line from another ion. Good diagnostic ratios in the transition region include the O IV lines at ~1400 Å which have been extensively studied from Skylab, SMM, UVSP and HRTS[57,58]. Since the spectral resolution of SUMER will be so much better than the previous instruments, it should be possible to explore more diagnostics below 1200 Å, including C III, N IV and O V lines from the Be-sequence, N III and Ne VI from the B-sequence, and Si III and S V from the Mg-sequence. SUMER will be somewhat restricted in its simultaneous wavelength coverage and observing sequences must be carefully designed to make maximum use of these electron density diagnostics. The lines from Mg VI and Si VIII should be particularly useful for coronal hole diagnostics and S X for the quiet Sun.

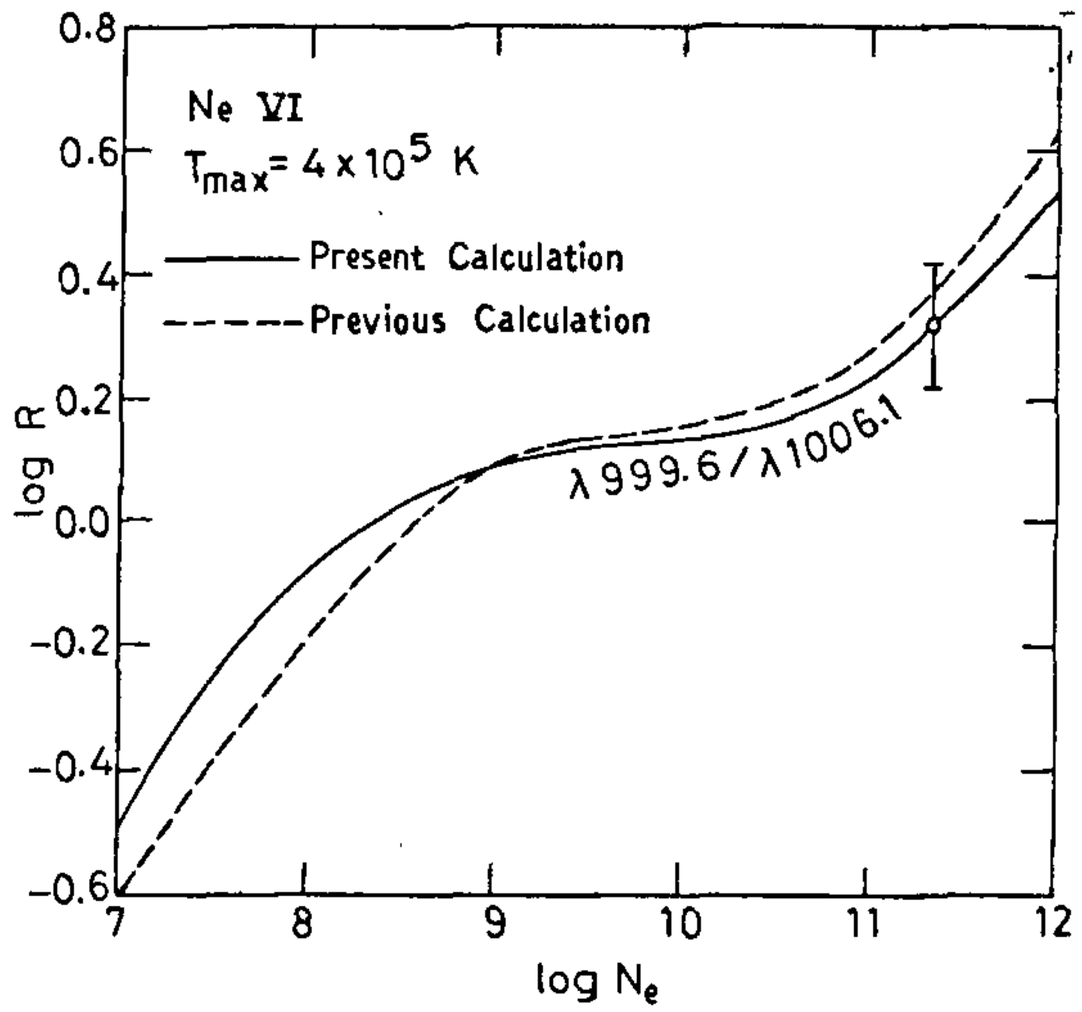


**Figure 5.** Ne VI $\lambda$999.6/$\lambda$1006.1 theoretical line-ratio at $T_{max} = 4 \times 10^5$ K as a function of electron density[27].

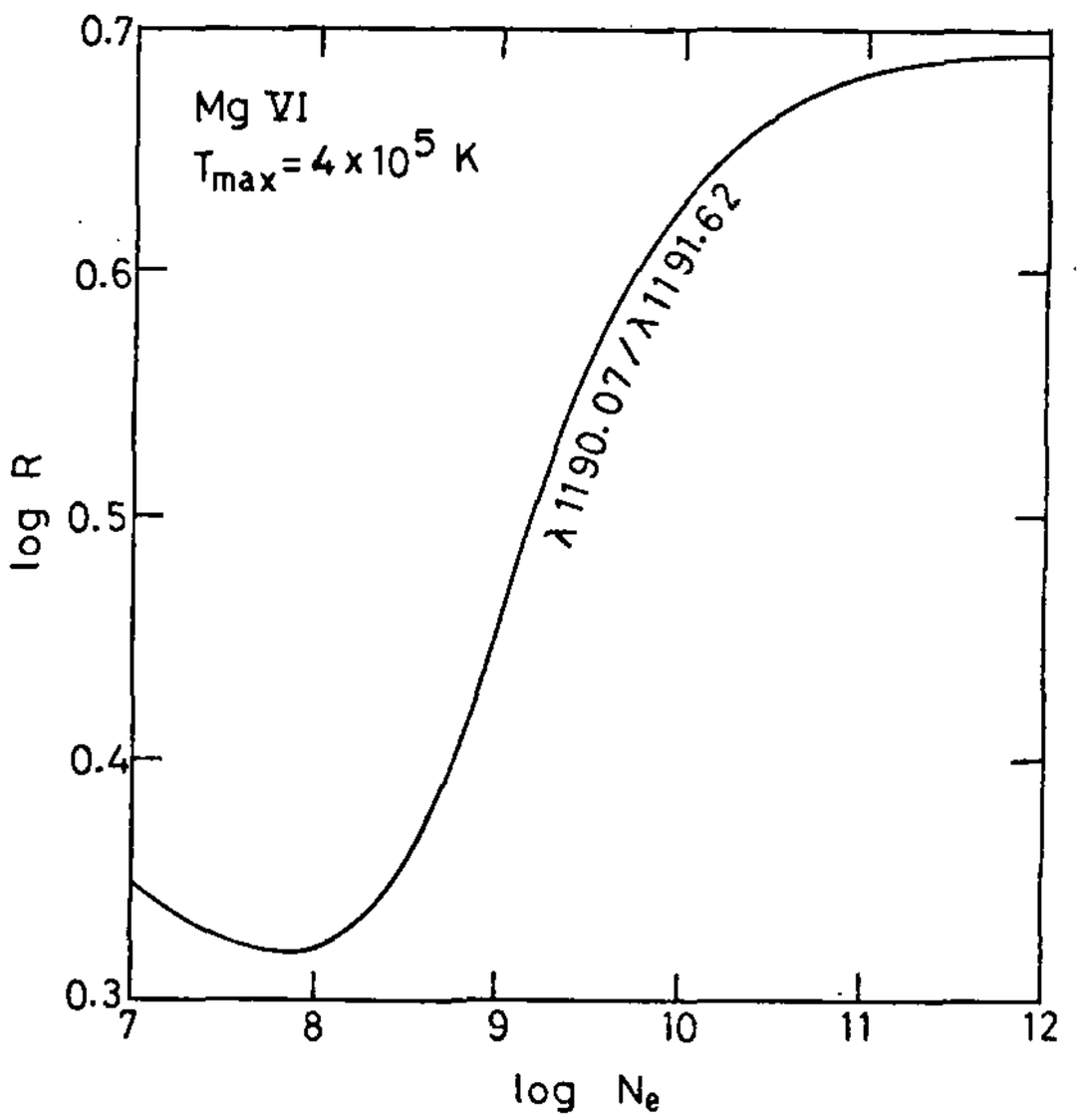


**Figure 6.** Mg VI $\lambda$1190.07/$\lambda$1191.62 theoretical line ratio at $T_{max} = 4 \times 10^5$ K as a function of electron density[27].

Studies proposed[59] for electron temperature determination include the lithium-like ion O VI $\lambda$1032/$\lambda$173 and $\lambda$1032/$\lambda$150. Other observational tests for non-equilibrium ionization due to flows in the transition region plasma have been suggested[60]. These include the temperature sensitive ratios of C IV $\lambda$1548/$\lambda$312, and O V $\lambda$629/$\lambda$172. It is hoped that these ratios will be used

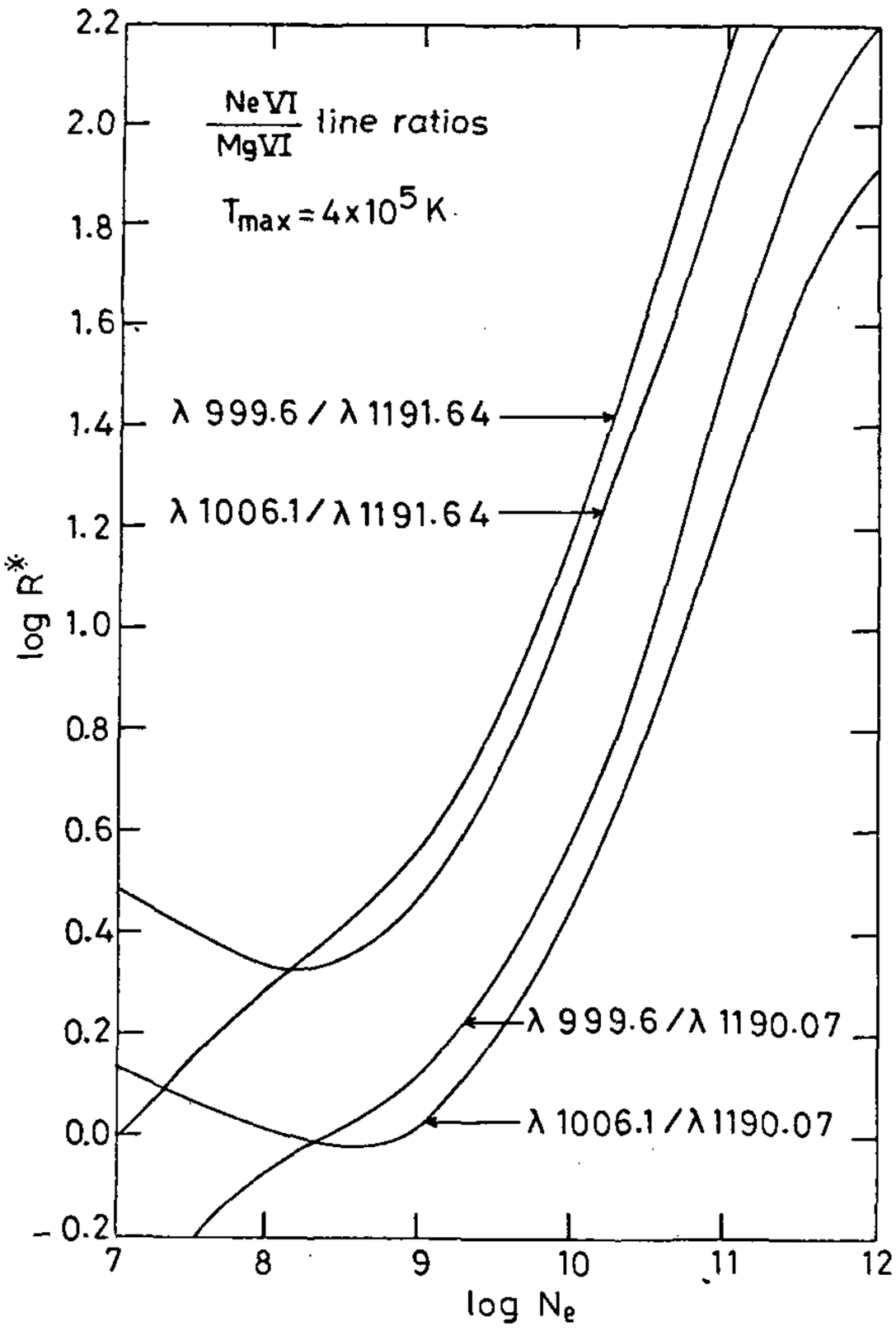


**Figure 7.** Normalized Ne VI/Mg VI theoretical line ratios at $T_{max} = 4 \times 10^5$ K as a function of electron density[27].

for studying coronal hole temperature distributions in a joint CDS-SUMER observation programme. Other possible SUMER line pairs, closer in wavelength, are C II $\lambda$1335/$\lambda$904, N III $\lambda$991/$\lambda$686, O III $\lambda$730/$\lambda$599, O IV $\lambda$790/$\lambda$544, Mg IX $\lambda$749/$\lambda$706 and S XI $\lambda$604/$\lambda$580. Dynamical studies will be of prime importance for SUMER. The studies with HRTS spectra are particularly relevant. Doppler motions and non-thermal broadenings will be measured over a large temperature range and with a high time resolution. The goal will be to distinguish between different models for coronal heating. For example, suggestion has been made to carry out some studies with SUMER of limb to disk spectral line widths to distinguish between different types of wave motion[61].

Finally, as discussed before, relative element abundances are found to vary in different regions of the solar atmosphere. The FIP-dependent element variation has also been shown from solar wind and spectroscopic studies (see Figure 3). The causes of these variations are poorly understood. In view of its importance for the understanding of physical processes in solar and cosmic plasmas, an observing sequence for SUMER[55] has been planned to investigate the upper transition region abundance variations and also electron densities by measuring the line intensity ratios of high-FIP coronal spectral lines (Ne VI: 999.6 and 1006.1 Å) to low-FIP ones (Mg VI: 1190.07 and 1191.62 Å). Since these lines are formed at nearly the same temperature of about $4 \times 10^5$ K, the effect of the solar differential emission measure on the line intensity ratio is minimized. In addition, Ne VI $\lambda$999.6/$\lambda$1006.1 and Mg VI $\lambda$1190.07/$\lambda$1191.62 line ratios as shown in Figures 5 and 6 respectively, are good density diagnostics for densities $>10^8$ cm$^{-3}$, applicable to active regions, sunspots, umbrae, and flare plasmas. Ne VI/Mg VI density-sensitive line ratios are shown in Figure 7. This sequence will probably work best for active and quiet regions, coronal holes, and prominences off-limb, because of the weakness of forbidden lines. The goal is to measure these forbidden lines in several different regions over a range of positions outside the limb, covering as large a range of heights as the count rates allow. The density obtained from the density-sensitive line ratios will be used to evaluate the Ne/Mg abundance ratio by making use of the Ne VI/Mg VI line intensity ratios in different regions of the solar atmosphere (see Figure 7).

## Concluding remarks

In conclusion, EUV diagnostic capabilities with the recent solar observations made from space and future high resolution EUV observations obtainable from the CDS and the SUMER instruments flown on board the SOHO mission present a powerful tool to better understanding of some of the tricks of our Sun, e.g., the existence of the corona and the acceleration of the solar wind. And the research investigations presented in this review describe how to achieve this goal by making a careful analysis of some of the prominent solar ions that are capable of probing the solar plasma, thereby providing some physical parameters crucial for understanding coronal physics and underlying mechanisms, e.g., plasma temperature, density, relative elemental abundances, column emission measures, etc. The scope is enormous for future investigations on this topic which concerns not only the Sun and other cosmic objects but also laboratory plasma such as laser-produced and tokamak.

1. Dere, K. P. and Mason, H. E., in *Solar Active Regions* (ed. Orrall, F. Q.), Colorado University Press, 1981, p. 129.
2. Doschek, G. A., in *Autoionization* (ed. Temkin, A.), Plenum, 1985, p. 171.
3. Dwivedi, B. N., *Space Sci. Rev.*, 1994, **65**, 289.
4. Mason, H. E. and Monsignori Fossi, B. C., *Astron. Astrophys. Rev.*, 1994, **6**, 123.
5. Arnaud, M. and Rothenflug, R., *Astron. Astrophys. Suppl.*, 1985, **60**, 425.

6. Arnaud, M. and Raymond, J. C., *Astrophys. J.*, 1992, **398**, 39.
7. Pottasch, S. R., *Space Sci. Rev.*, 1964, **3**, 816.
8. Monsignori Fossi, B. C. and Landini, M., *Adv. Space Res.*, 1991, **1**, 281.
9. Harrison, R. A. and Thompson, A. M., *RAL-91-092*, 1992.
10. Monsignori Fossi, B. C., Landini, M., Del Zanna, G. and Drake, I. J. S., Preprint (1994).
11. Meyer, J. P., *Astrophys. J. Suppl.*, 1985, **57**, 151.
12. Meyer, J. P., *Adv. Space Res.*, 1991, **11**, 269.
13. Meyer, J. P., *Adv. Space Res.*, 1993, **13**, 377.
14. Widing, K. G. and Feldman, U., in *Solar Wind Seven* (eds Marsch, E. and Schwenn, R.), COSPAR Colloquia Series, 1992, vol. 3, p. 405.
15. Cook, J. W., Cheng, C. C., Jacobs, V. L. and Antiochos, S. K., *Astrophys. J.*, 1989, **338**, 1176.
16. Sutherland, R. A. and Dopita, M. A., *Astrophys. J. Suppl.*, 1993, **88**, 253.
17. Dere, K. P. and Mason, H. E., *Solar Phys.*, 1993, **144**, 217.
18. Mason, H. E., Bhatia, A. K., Kastner, S. O., Neupert, W. M. and Swartz, M., *Solar Phys.*, 1984, **92**, 199.
19. Conlon, E. S., Keenan, F. P. and Aggarwal, K. M., *Phys. Scr.*, 1992, **46**, 518.
20. Noyes, R. W., in *Physics of the Solar Corona* (ed. Macris, C. J.), D. Reidel, 1971, p. 192.
21. Kastner, S. O., Rothe, E. D. and Neupert, W. M., *Astron. Astrophys.*, 1976, **53**, 203.
22. Kastner, S. O. and Mason, H. E., *Astron. Astrophys.*, 1978, **67**, 119.
23. Hansen, E. and Schaffner, S. (eds), Proceedings of the November 7–10, 1977 OSO-8 Workshop, Univ. of Colorado.
24. Bruner, M. E. and McWhirter, R. W. P., *Astrophys. J.*, 1979, **231**, 557.
25. Feldman, U., *Phys. Scr.*, 1992, **46**, 202.
26. Feldman, U. and Widing, K. G., *Astrophys. J.*, 1993, **414**, 381.
27. Dwivedi, B. N. and Mohan, A., *Solar Phys.*, 1995, **157**, 135.
28. Vernazza, J. E. and Mason, H. E., *Astrophys. J.*, 1978, **226**, 720.
29. Dwivedi, B. N. and Raju, P. K., *Solar Phys.*, 1980, **68**, 111.
30. Dwivedi, B. N., *Solar Phys.*, 1988, **116**, 405.
31. Dwivedi, B. N. and Gupta, A. K., *Solar Phys.*, 1991, **135**, 415.
32. Dwivedi, B. N. and Mohan, A., *Solar Phys.*, 1995, **156**, 197.
33. Dwivedi, B. N., Mohan, A. and Gupta, A. K., *Solar Phys.*, 1995, **161**, 241.
34. Keenan, F. P., Conlon, E. S., Bowden, D. A., Dwivedi, B. N. and Widing, K. G., *Solar Phys.*, 1994, **149**, 137.
35. Keenan, F. P. and Warren, G. A., *Solar Phys.*, 1993, **146**, 19.
36. Doyle, J. G. and McWhirter, R. W. P., *Mon. Not. R. Astron. Soc.*, 1980, **193**, 947.
37. Feldman, U., Doschek, G. A., Mariska, J. T., Bhatia, A. K. and Mason, H. E., *Astrophys. J.*, 1978, **226**, 674.
38. Dwivedi, B. N. and Raju, P. K., *Adv. Space Res.*, 1988, **8**, 179.
39. Dwivedi, B. N., *Solar Phys.*, 1991, **131**, 49.
40. Doschek, G. A., *Astrophys. J.*, 1984, **279**, 446.
41. Almleaky, Y. M., Brown, J. C. and Sweet, P. A., *Astron. Astrophys.*, 1989, **224**, 328.
42. Dwivedi, B. N., in *Basic Plasma Processes on the Sun* (eds Priest, E. R. and Krishan, V.), Kluwer Academic Publishers, 1990, p. 403.
43. Brown, J. C., Dwivedi, B. N., Almleaky, Y. M. and Sweet, P. A., *Astron. Astrophys.*, 1991, **249**, 277.
44. Vernazza, J. E. and Reeves, E. M., *Astrophys. J. Suppl.*, 1978, **37**, 485.
45. Neupert, W. M., Epstein, G. L., Thomas, R. J. and Thompson, W. T., *Solar Phys.*, 1992, **137**, 87.
46. Thomas, R. J. and Neupert, W. M., *Astrophys. J. Suppl.*, 1994, **91**, 461.
47. Brickhouse, N. S., Raymond, J. C. and Smith, B. W., *Astrophys. J. Suppl.*, 1995, **97**, 551.
48. Brosius, J. W., Davila, J. M., Thomas, R. J. and Thompson, W. T., *Astrophys. J.*, 1994, **425**, 343.
49. Dwivedi, B. N. and Mohan, A., *Solar Phys.*, 1995, **156**, 81.
50. Jordan, S. D., Thompson, W. T., Thomas, R. J. and Neupert, W. M., *Astrophys. J.*, 1993, **406**, 346.
51. Dwivedi, B. N., Mohan, A. and Thomas, R. J., 1996, paper in preparation.
52. Harrison, R. A. *et al.*, *Solar Phys.*, 1995, **162**, 233.
53. Wilhelm, K. *et al.*, *Solar Phys.*, 1995, **162**, 189.
54. Harrison, R. A., *The Coronal Diagnostic Spectrometer for SOHO*, CDS-Scientific Report, SC-CDS-RAL-SN-95-0001, Blue Book, 1995.
55. Wilhelm, K., *The SUMER Spectometer for SOHO*, Scientific Report, SUM-MPAE-RO-113000-03-1, 1995, vol. 3.02, Red Book.
56. Dere, K. P., Mason, H. E., Widing, K. G. and Bhatia, A. K., *Astrophys. J. Suppl.*, 1979, **40**, 341.
57. Dwivedi, B. N. and Gupta, A. K., *Solar Phys.*, 1992, **138**, 283.
58. Dwivedi, B. N., *Solar Phys.*, 1994, **154**, 397.
59. Haug, E., *Solar Phys.*, 1991, **136**, 111.
60. Spadaro, D., Leto, P. and Antiochos, S. K., in Proceedings of the Second SOHO Workshop, Elba, 1994.
61. McClements, K. G., Harrison, R. A. and Alexander, D. A., *Solar Phys.*, 1991, **131**, 41.


ACKNOWLEDGEMENTS. We thank the editor and an anonymous referee for helpful comments.

Received 28 December 1995; revised accepted 8 March 1996